



**Effects of Cylindrical Chopper Geometry on Calculating
Power Coupling Efficiency and Noise Equivalent
Temperature Difference**

by Abigail S. Hedden, Charles C. Dietlein, and David A. Wikner

ARL-TR-5428

January 2011

NOTICES

Disclaimers

The findings in this report are not to be construed as an official Department of the Army position unless so designated by other authorized documents.

Citation of manufacturer's or trade names does not constitute an official endorsement or approval of the use thereof.

Destroy this report when it is no longer needed. Do not return it to the originator.

Army Research Laboratory

Adelphi, MD 20783-1197

ARL-TR-5428

January 2011

Effects of Cylindrical Chopper Geometry on Calculating Power Coupling Efficiency and Noise Equivalent Temperature Difference

Abigail S. Hedden, Charles C. Dietlein, and David A. Wikner
Sensors and Electron Devices Directorate, ARL

REPORT DOCUMENTATION PAGE

Form Approved
OMB No. 0704-0188

Public reporting burden for this collection of information is estimated to average 1 hour per response, including the time for reviewing instructions, searching existing data sources, gathering and maintaining the data needed, and completing and reviewing the collection information. Send comments regarding this burden estimate or any other aspect of this collection of information, including suggestions for reducing the burden, to Department of Defense, Washington Headquarters Services, Directorate for Information Operations and Reports (0704-0188), 1215 Jefferson Davis Highway, Suite 1204, Arlington, VA 22202-4302. Respondents should be aware that notwithstanding any other provision of law, no person shall be subject to any penalty for failing to comply with a collection of information if it does not display a currently valid OMB control number.

PLEASE DO NOT RETURN YOUR FORM TO THE ABOVE ADDRESS.

1. REPORT DATE (DD-MM-YYYY) January 2011	2. REPORT Summary	3. DATES COVERED (From - To) October 2010			
4. TITLE AND SUBTITLE Effects of Cylindrical Chopper Geometry on Calculating Power Coupling Efficiency and Noise Equivalent Temperature Difference		5a. CONTRACT NUMBER			
		5b. GRANT NUMBER			
		5c. PROGRAM ELEMENT NUMBER			
6. AUTHOR(S) Abigail S. Hedden, Charles C. Dietlein, and David A. Wikner		5d. PROJECT NUMBER			
		5e. TASK NUMBER			
		5f. WORK UNIT NUMBER			
7. PERFORMING ORGANIZATION NAME(S) AND ADDRESS(ES) U.S. Army Research Laboratory ATTN: RDRL-SER-M 2800 Powder Mill Road Adelphi, MD 20783-1197		8. PERFORMING ORGANIZATION REPORT NUMBER ARL-TR-5428			
9. SPONSORING/MONITORING AGENCY NAME(S) AND ADDRESS(ES)		10. SPONSOR/MONITOR'S ACRONYM(S)			
		11. SPONSOR/MONITOR'S REPORT NUMBER(S)			
12. DISTRIBUTION/AVAILABILITY STATEMENT Approved for public release; distribution unlimited.					
13. SUPPLEMENTARY NOTES					
14. ABSTRACT This report explores the geometrical effects of a cylindrical chopper wheel on calculations of power coupling efficiency and noise equivalent temperature difference (NETD) of array elements. The overall efficiency of the cylindrical chopper wheel is found to be about 53% from geometrical arguments. In the limit that a detector beam fills the chopper aperture, if this efficiency is not accounted for, it can lead to detector NETD values that are a factor of 1.9 too high when calculated using standard double-modulation measurement techniques. For the particular geometry used with this setup, a power coupling efficiency of 78% was calculated for typical detector elements, resulting in values of detector NETD that were too large by a factor of 1.3 when the coupling efficiency was unaccounted for. This factor plays a role in accounting for some of the discrepancy between NETD values calculated based on diode sensitivity estimates and NETDs measured for individual array elements using double-modulation measurements.					
15. SUBJECT TERMS Millimeter-wave measurements, millimeter-wave technology, planar arrays					
16. SECURITY CLASSIFICATION OF:			17. LIMITATION OF ABSTRACT UU	18. NUMBER OF PAGES 18	19a. NAME OF RESPONSIBLE PERSON Abigail S. Hedden
a. REPORT Unclassified	b. ABSTRACT Unclassified	c. THIS PAGE Unclassified			19b. TELEPHONE NUMBER (Include area code) (301) 394-0877

Contents

List of Figures	iv
Summary	1
1. Introduction	3
2. Methods, Assumptions, and Procedures	4
3. Results and Discussion	6
4. Conclusions	9
5. References	10
List of Symbols, Abbreviations, and Acronyms	11
Distribution List	12

List of Figures

- Figure 1. Diagram showing a side view of the ARL mm-wave array, cylindrical optical chopper (metal blades are shown toward the top and bottom), and the scene being imaged.....4
- Figure 2. Normalized total projected height of the scene (solid line) as dictated by the array's cylindrical chopper geometry compared with a perfect chopper (dashed line) as a function of rotation angle ϕ . Areas under each curve from $\phi = 0^\circ$ and 90° are indicated.5
- Figure 3. Angles between the detector array and chopper blades with respect to the line-of-sight axis for the particular geometry used with the ARL array. θ_{tot} represents the total angle subtended by the scene visible to the detectors as the chopper rotates a complete revolution.7
- Figure 4. (Left) Normalized angle θ_{tot} for the ARL array cylindrical chopper (solid line) and a perfect chopper wheel (dashed line); the angular efficiency is $\sim 80\%$. (Right) Principal plane copolar radiation power pattern for a typical ARL array diagonal horn antenna. Note that the normalized angle is: $u/\pi = (d/\lambda) \sin \delta$. Since $d/\lambda = 3$, the range corresponds to $\delta = 0 - 90^\circ$7
- Figure 5. Power coupling efficiency, R , for a typical array horn antenna for the setup described in this work is shown as a function of rotation angle ϕ over a half period of the chopper wheel. The overall power coupling efficiency is 78% compared with a perfect chopper.....9

Summary

This report explores the geometrical effects of a cylindrical chopper wheel on calculations of power coupling efficiency and noise equivalent temperature difference (NETD) of array elements. The overall efficiency of the cylindrical chopper wheel is found to be about 53% from geometrical arguments. In the limit that a detector beam fills the chopper aperture, if this efficiency is not accounted for, it can lead to detector NETD values that are a factor of 1.9 too high when calculated using standard double-modulation measurement techniques. For the particular geometry used with this setup, a power coupling efficiency of 78% was calculated for typical detector elements, resulting in values of detector NETD that were too large by a factor of 1.3 when the coupling efficiency was unaccounted for. This factor plays a role in accounting for some of the discrepancy between NETD values calculated based on diode sensitivity estimates and NETDs measured for individual array elements using double-modulation measurements.

INTENTIONALLY LEFT BLANK.

1. Introduction

We consider the effects of optical chopper geometry on calculations of power coupling efficiency and NETD of detector elements in the U.S. Army Research Laboratory's (ARL) 32-pixel Linear Millimeter-wave Array. We briefly summarize the relevant properties of the array pertaining to this setup. An overview of the array, the cylindrical chopper, and its geometry are presented in reference 1. The instrument is a 32-channel, zero-bias, room temperature detector array designed for operation in the 80–140 GHz range for passive millimeter-wave (mm-wave) imaging applications. At its heart, it incorporates antimony (Sb)-heterostructure backward tunnel diodes (BTDs) fabricated on gallium arsenide (GaAs) substrates that were developed at HRL Laboratories (2) as low-noise, low-cost mm-wave imaging sensors capable of high sensitivity, room temperature operation as part of the Defense Advanced Research Projects Agency (DARPA) Microantenna Arrays: Technology and Applications (MIATA) program (3). In order to achieve a good match with minimal losses over a 60-GHz bandwidth, BTDs were flip-chip mounted to quartz substrates with the detector chip located inside of the horn antenna output waveguide sections. Diagonal horns with cylindrical ridged waveguide outputs were used to achieve the large operational bandwidth, and coupling to the waveguide was accomplished via E-plane probes patterned on the quartz chip (4).

The low-noise and zero-bias characteristics of these detectors alleviate the need for signal pre-amplification and bias-routing circuitry, greatly simplifying the overall array architecture. The zero-bias diodes are limited by thermal (Johnson) noise and are free from both 1/f and shot noise. Since low signal levels and high noise remain significant challenges for room temperature passive mm-wave and terahertz (THz) imaging, the sensitive, low-noise performance of the diode detectors was a key consideration of the array design. To reduce the overall noise and enable synchronous detection of the array output, a long cylindrical chopper wheel was designed to optically chop the imaged scene. Ultra-low-noise readout electronics compatible with room temperature video-rate passive imaging applications were designed for use with the array/chopper wheel system (5). In this work, we explore the effects of the cylindrical chopper geometry on calculations of detector power coupling efficiency and NETD. An overview of the cylindrical chopper and its potential limitations is presented in section 2. Section 3 addresses detector power coupling efficiency and its effect on NETD calculations specific to the geometry of this experiment and a brief summary of these results is presented in section 4.

2. Methods, Assumptions, and Procedures

Figure 1 shows a side-view diagram of the chopper relative to the detector elements and the scene being imaged. The chopper wheel consists of a rotating metal half-cylinder that has been anodized. The two quarter sections of the half-cylinder are located 180° apart so that, in the orientation shown in figure 1 with solid lines, the linear array has a maximally unobstructed view of the scene. The chopper blades are located at the top and bottom of the figure in this case. The metal half-cylinder chopper is a single rigid body of radius 5 cm ($R_i = 4.84$ cm) that pivots about a central axis and may be driven at frequencies in excess of 50 Hz by a motor. The array line of sight is coincident with the central axis of the chopper. Let ϕ be the angle between the line of sight and the chopper blade as shown in figure 1 as the chopper spins in a counterclockwise direction from $\phi = 0^\circ$. Note that the projected height of the scene visible from the array varies with ϕ as the chopper wheel turns and is represented in the diagram as h . The maximum viewable height of the scene occurs in the orientation shown by solid lines in figure 1, where $\phi = \phi_0$ and $h = h_{\max}$, and is equal to $2 h_{\max}$. Because each metal section of the chopper subtends 90° , $\phi_0 = 45^\circ$. Expressions for h and h_{\max} are as follows:

$$h = R_i \cdot \sin \phi \quad \text{and} \quad h_{\max} = R_i \cdot \sin \phi_0 \quad (1)$$

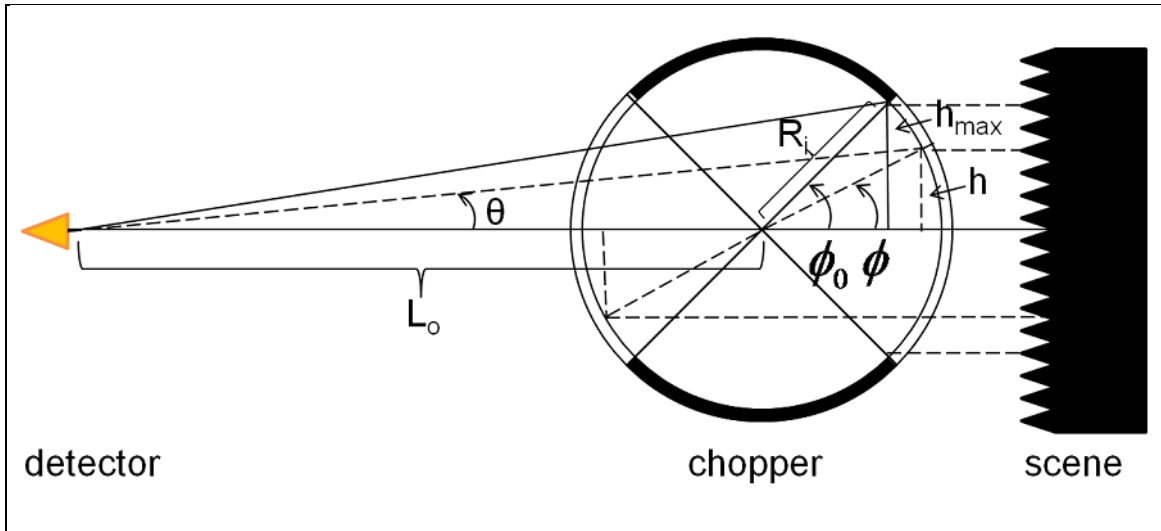


Figure 1. Diagram showing a side view of the ARL mm-wave array, cylindrical optical chopper (metal blades are shown toward the top and bottom), and the scene being imaged.

Figure 2 was generated from equation 1 and shows the normalized projected height, $h_{\text{tot}}/(2h_{\max})$, of the scene that is visible to the detector as the chopper turns counterclockwise one complete revolution. As shown in the figure, h_{tot} represents the total projected height above and below the line of sight drawn in figure 1 and the chopper revolution begins at $\phi = 0^\circ$. As the chopper wheel rotates counterclockwise from a fully closed position at $\phi = 0^\circ$ to ϕ_0 , the total projected height

increases to its maximum value. Rotating from $\phi = \phi_0$ to $2\phi_0$, the falling edge of the top blade and the rising edge of the bottom blade of the chopper begin to occult the visible scene until the chopper is again fully closed. The scene remains fully occulted until the cycle repeats with a period of 180° . The resulting triangular-shaped total projected height curve is shown in figure 2 (solid contour) over one full revolution of the chopper wheel. For comparison, the results of a perfect chopper (one which chops between the reference and scene instantaneously) are shown in dashed contours. Figure 2 indicates that, unlike the perfect chopper, the duty cycle of the array chopper wheel is about 25%. Between $\phi = 0^\circ$ and 90° and again between $\phi = 180^\circ$ and 270° , the total projected view visible through the chopper contains both the chopper blades and the scene (with temperatures $T_{chopper}$ and T_{scene} , respectively). This can be thought of as a scene with a temperature dependant on how much of the scene is occulted by the chopper as the wheel rotates through half a period (90°). The effective temperature of the scene is related to the ratio of areas under the curves shown in figure 2 by the following:

$$T_{eff} = T_{chopper}[1 - (A_h/A_{tot})] + T_{scene} (A_h/A_{tot}) \quad (2)$$

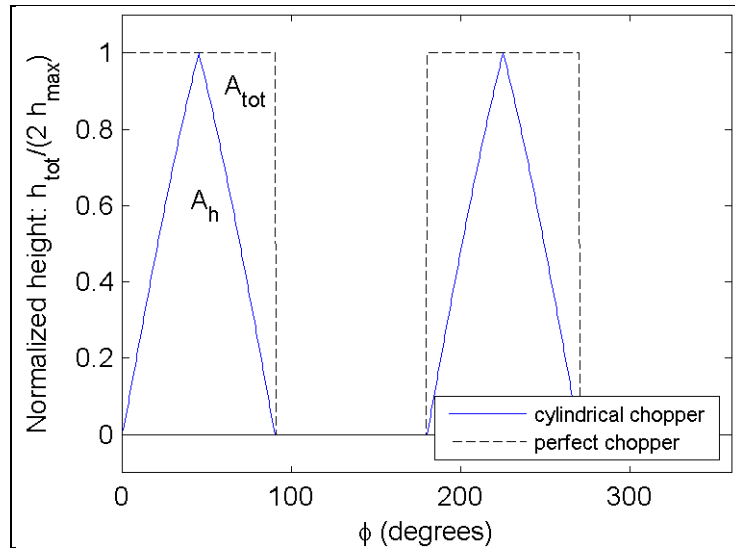


Figure 2. Normalized total projected height of the scene (solid line) as dictated by the array's cylindrical chopper geometry compared with a perfect chopper (dashed line) as a function of rotation angle ϕ . Areas under each curve from $\phi = 0^\circ$ and 90° are indicated.

Standard numerical integration techniques were used to compute the area under the curve of projected height in figure 2, A_h , resulting in $A_h/A_{tot} = 53\%$. For chopper and scene temperatures of 295 and 77 K, respectively, this results in $T_{eff} = 180$ K. Instead of observing an effective temperature difference of 218 K between the chopper and cold scene, a 115 K temperature difference ($295 \text{ K} - T_{eff}$) results for the cylindrical chopper. Depending on the specifics of the setup, including the location of the detector array (L_0) and chopper geometry (R_i), this will lead to detector beam coupling efficiencies that are lower and calculations of NETD that are

correspondingly higher if geometric effects are unaccounted for. In the limit where a detector beam fills the chopper aperture, standard double-modulation measurement techniques result in NETD calculations that are a factor of 1.9 too high, since NETD is directly proportional to temperature difference.

3. Results and Discussion

For the particular configuration used with the ARL array, L_0 and R_i are 8 and 4.84 cm, respectively. Using equation 1 and figure 1, the angle between the line-of-sight axis and the chopper blade edge, θ , is expressed as follows:

$$\theta = \sin^{-1}[(R_i \sin \phi) / \sqrt{(L_0 + R_i \cos \phi)^2 + (R_i \sin \phi)^2}] \quad (3)$$

Four such angles can be simultaneously described because there are four blade edges. Let θ_{top} and θ_{bottom} represent the minimum angles (in absolute value) defined above and below the line-of-sight axis by the edges as the chopper rotates; θ_{tot} is the total angle, $\theta_{tot} = \theta_{top} + |\theta_{bottom}|$. Figure 3 shows all three of these curves, θ_{top} , θ_{bottom} , and θ_{tot} , as a function of ϕ over one complete rotation of the chopper wheel. Figure 4 (left) shows a comparison between normalized θ_{tot} for the chopper geometry used with the ARL array and what would be expected from a perfect chopper. The angular efficiency is described by the ratio of the areas under both curves shown in figure 4 (left) over half a period ($\phi = 0^\circ$ to 90° , for example) and is about 80%. In order to relate this result back to NETD, θ_{tot} is used to calculate the power coupling to a typical array element feed horn.

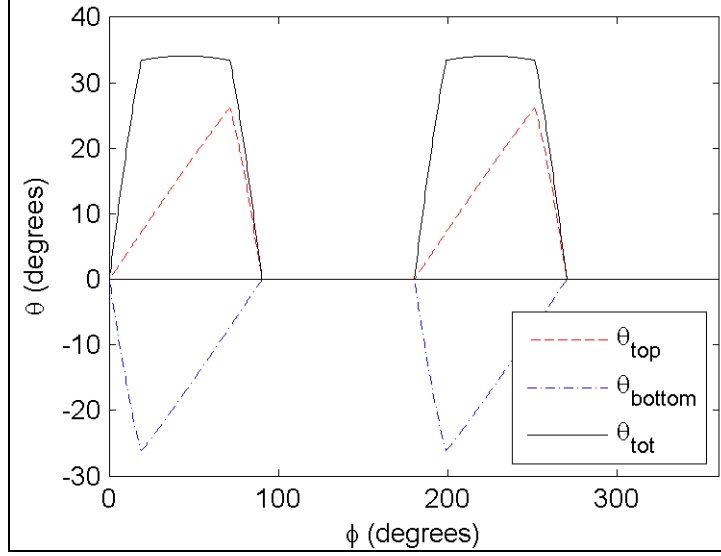


Figure 3. Angles between the detector array and chopper blades with respect to the line-of-sight axis for the particular geometry used with the ARL array. θ_{tot} represents the total angle subtended by the scene visible to the detectors as the chopper rotates a complete revolution.

Note: θ_{bottom} values are shown as negative numbers.

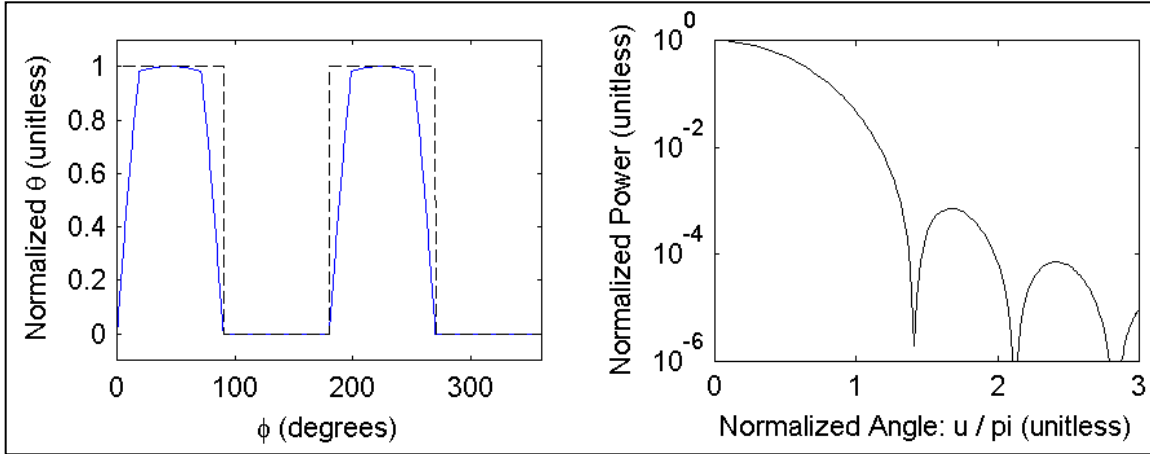


Figure 4. (Left) Normalized angle θ_{tot} for the ARL array cylindrical chopper (solid line) and a perfect chopper wheel (dashed line); the angular efficiency is $\sim 80\%$. (Right) Principal plane copolar radiation power pattern for a typical ARL array diagonal horn antenna. Note that the normalized angle is $u/\pi = (d/\lambda) \sin \delta$. Since $d/\lambda = 3$, the range corresponds to $\delta = 0 - 90^\circ$.

Power patterns for a typical ARL array diagonal horn antenna were calculated from expressions for the principal plane copolar electric field (θ):

$$E_{co} = \frac{\sin u/\sqrt{2}}{u/\sqrt{2}} \cdot \frac{\cos u/\sqrt{2}}{1 - (2u^2/\pi^2)} \quad (4)$$

Note that the principal plane cross-polar field is 0, d is the length of the sides of the diagonal horn aperture, $u = (\pi d/\lambda) \sin \delta$, and for the array horn antennas used in this work, $d/\lambda = 3$. Using equation 4, the normalized copolar radiation power pattern was calculated and plotted in figure 4 (right) as a function of angle δ with respect to the principle axis of the horn antenna from $\delta = 0^\circ$ (on-axis) to $\delta = 90^\circ$ (corresponding to a range of $u/\pi = 0 - 3$). Note that the normalized power pattern is symmetric with respect to the horizontal axis. This power pattern is used in conjunction with figure 3 to determine the power coupling efficiency. The coupling efficiency is the ratio of the total integrated power pattern over the angular region containing the visible scene (θ_{bottom} to θ_{top}) to the total power calculated over the maximally visible scene (e.g., what would be expected from a perfect chopper). The resulting power coupling ratio for any chopper rotation angle ϕ is given by the following expression:

$$R(\phi) = \frac{\int_{\delta_0=\theta_{bottom}}^{\delta_1=\theta_{top}} E_{co}^2(\delta) d\delta}{\int_{-90^\circ}^{90^\circ} E_{co}^2(\delta) d\delta} \quad (5)$$

Note that for any angle ϕ , values of θ are determined using equation 3 for each edge of the chopper blade and that θ_{bottom} and θ_{top} are shown in figure 3 as a function of ϕ . Note that for a setup including a perfect chopper, the entire scene is visible and the total integrated power calculated is a constant. The power coupling ratio equation 5 was used along with figures 3 and 4 to find the total normalized power coupling for a typical array element horn antenna for the setup used in this experiment as a function of chopper rotation angle, ϕ . The results are shown in figure 5. This figure shows the calculation of power coupling ratio equation 5 over a quarter revolution (half-period) of the chopper wheel, $\phi = 0^\circ$ to 90° and the area beneath the curve describes the total power coupling efficiency for typical elements of the ARL linear array. The resulting power coupling efficiency was found by numerical integration techniques and is 78%, similar to the 80% angular efficiency calculated previously. Since the ARL array elements are square-law detectors, their signal is proportional to the total incident power of the scene and the power coupling efficiency. Standard double-modulation techniques, where detector response is recorded while room temperature and liquid nitrogen cooled loads are alternately placed in front of the chopper wheel, were used to calculate detector NETD. NETD values determined by this method are inversely proportional to the power coupling efficiency. In other words, a 78% power coupling efficiency results in NETD calculations that are too large by a factor of about 1.3 if power coupling efficiency is not properly accounted for and a perfect chopper is assumed instead.

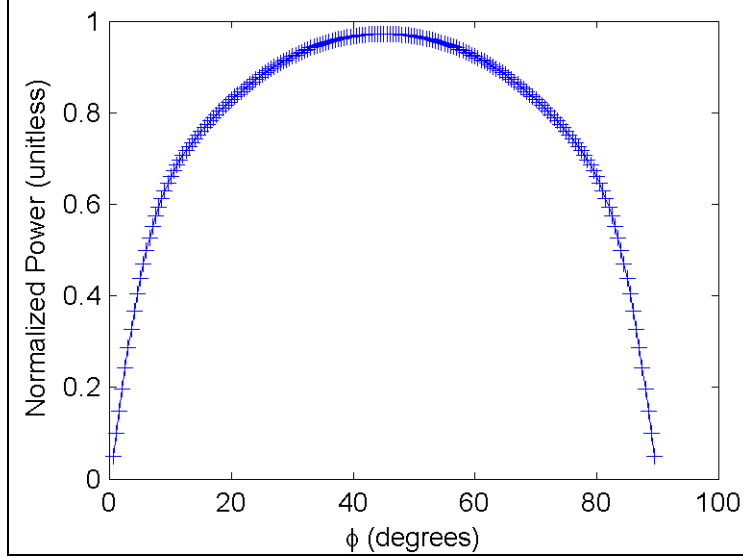


Figure 5. Power coupling efficiency, R , for a typical array horn antenna for the setup described in this work is shown as a function of rotation angle ϕ over a half period of the chopper wheel. The overall power coupling efficiency is 78% compared with a perfect chopper.

4. Conclusions

In summary, we have calculated the efficiency of the cylindrical chopper wheel currently being used with the ARL 32-pixel Linear Millimeter-wave Array and determined its effects on power coupling and calculated values of NETD for typical array elements. From geometrical arguments, we find that the overall efficiency of the cylindrical chopper wheel is about 53%. Standard double-modulation measurement techniques result in NETD calculations that are too large if this efficiency is unaccounted for. For example, in the limit where the detector field of view spans entire chopper aperture, NETD calculations determined by this method are too large by a factor of 1.9. For the particular system geometry and array element horn antennas used in this setup, we calculate an overall power coupling efficiency of 78% for typical array elements. Double-modulation measurements made with the current array/chopper wheel configuration result in NETD calculations that are correspondingly too high by a factor of 1.3.

5. References

1. Wikner, D. A.; Grossman, E. N. Demonstration of a Passive, Low Noise, Millimeter-wave Detector Array for Imaging. *Proc. SPIE* **2009**, 7309, 730909-1–730909-6.
2. Schulman, J. N.; Croke, E. T.; Chow, D. H.; Dunlap, H. L.; Holabird, K. S.; Morgan, M. A.; Weinreb, S. Quantum Tunneling Sb-heterostructure Millimeter-wave Diodes. *IEDM Tech. Digest* **2001**, 765–767.
3. Stickley, C. M.; Filipkowski, M. E. Microantenna Arrays: Technology and Applications (MIATA)—an overview. *Proc. SPIE* **2004**, 5619, 47–58.
4. Moyer, H. P.; Bowen, R. L.; Schulman, J. N.; Chow, D. H.; Thomas III, S.; Lynch, J. J.; Holabird, K. S. Sb-heterostructure Low Noise W-band Detector Diode Sensitivity Measurements. Microwave Symposium Digest, 2006. IEEE MTT-S, pp. 826–829, June 2006.
5. Chisum, J. D.; Grossman, E. N.; Popović, Z. Ultra-low Noise Readout Electronics for THz Imaging Arrays. In preparation.
6. Johnson, R. C.; Jasik, H. *Antenna Engineering Handbook*; 2nd Ed., McGraw-Hill Book Co., New York, 1984, ch. 15-4.

List of Symbols, Abbreviations, and Acronyms

ARL	U.S. Army Research
BTDs	backward tunnel diodes
DARPA	Defense Advanced Research Projects Agency
GaAs	gallium arsenide
MIATA	Microantenna Arrays: Technology and Applications
NETD	noise equivalent temperature difference
Sb	antimony

NO. OF COPIES	ORGANIZATION
1 ELEC	ADMNSTR DEFNS TECHL INFO CTR ATTN DTIC OCP 8725 JOHN J KINGMAN RD STE 0944 FT BELVOIR VA 22060-6218
1 CD	OFC OF THE SECY OF DEFNS ATTN ODDRE (R&AT) THE PENTAGON WASHINGTON DC 20301-3080
1	US ARMY INFO SYS ENGRG CMND ATTN AMSEL IE TD A RIVERA FT HUACHUCA AZ 85613-5300
1	COMMANDER US ARMY RDECOM ATTN AMSRD AMR W C MCCORKLE 5400 FOWLER RD REDSTONE ARSENAL AL 35898-5000
1	US ARMY RSRCH LAB ATTN RDRL CIM G T LANDFRIED BLDG 4600 ABERDEEN PROVING GROUND MD 21005-5066
8	US ARMY RSRCH LAB ATTN IMNE ALC HRR MAIL & RECORDS MGMT ATTN RDRL CIM L TECHL LIB ATTN RDRL CIM P TECHL PUB ATTN RDRL SER M A HEDDEN ATTN RDRL SER M C DIETLEIN ATTN RDRL SER M D WIKNER ATTN RDRL SER M E ADLER ATTN RDRL SER P AMIRTHARAJ ADELPHI MD 20783-1197
2	UNIV. OF COLORADO AT BOULDER DEPT ELEC CMPTR ENRGY ENG ATTN J CHISUM ATTN Z POPOVIC 425 UCB BOULDER, CO 80309-0245
1	OPTOELECTRONICS DIVISION, NATIONAL INSTITUTE OF STANDARDS AND TECHNOLOGY ATTN E GROSSMAN MAILCODE 815.04: 325 BROADWAY BOULDER, CO 80305

TOTAL: 16 (1 ELEC, 1 CD, 14 HCS)